EUROPEAN FUSION DEVELOPMENT AGREEMENT

EFDA–JET–CP(01)08-06

D.Borba, H.L.Berk, B.N.Breizman, A.Fasoli,
F.Nabais, S.D.Pinches, S.E.Sharapov, D.Testa
and JET EFDA Contributors

Modelling of Alfvén Waves in JET Plasmas with the CASTOR-K Code

Modelling of Alfvén Waves in JET Plasmas with the CASTOR-K Code

D.Borba[1,2], H.L.Berk[3], B.N.Breizman[3], A.Fasoli[4],
F.Nabais[1], S.D.Pinches[5], S.E.Sharapov[6], D.Testa[4]
and JET EFDA Contributors

[1]Associacão EURATOM/IST, Av. Rovisco Pais, 1049-001 Lisboa, Portugal
[2]EDFA Close Support Unit, Culham Science Centre, Abingdon, OX14 3DB UK
[3]Institute for Fusion Studies, University of Texas at Austin, Austin, Texas 78712 USA
[4]Plasma Science and Fusion Centre, MIT, Cambridge, Massachusetts MA02139 USA
[5]Max-Planck Institut fur Plasmaphysik, Euratom Association, Garching D85748, Germany
[6]Euratom/UKAEA Fusion Association, Culham Science Center, Abingdon, OX14 3DB, UK
**See Annex of J. Pamela et al., "Overview of Recent JET Results and Future Perspectives", Fusion Energy 2000 (Proc. 18th Int. Conf. Sorrento, 2000), IAEA, Vienna (2001).*

Preprint of Paper to be submitted for publication in Proceedings of the
7th IAEA TCM on Energetic Particles,
(Gothenburg, 8-11 October 2001)

ABSTRACT

A hybrid MHD-gyrokinetic model CASTOR-K developed for the study of AE stability in the presence of energetic ions has been applied to the interpretation of recent measurements of Alfvén waves in JET. These include the detailed AE damping measurements performed using the AE antenna excitation system and also the observations of Alfvén cascades in strongly reversed shear scenarios at JET. The mode conversion between the AEs and kinetic Alfvén waves and the relation to the Alfvén continuum is studied and the calculated damping is compared with the experimental data. The contribution of ICRH driven minority ions in the potential energy of the novel-type energetic particle mode localised around the point of zero magnetic shear is calculated. This mode is shown to be clearly linked to the ideal MHD "Alfvén continuum", computed with the CSCAS code and consistent with the observation of a quasi-periodic pattern of upward frequency sweeping Alfvén Cascades in JET.

1. INTRODUCTION

The study and the understanding of plasma instabilities is of great importance for the optimisation of the design and future operation of a fusion tokamak reactor[1]. Alfvén instabilities are particularly important, due to the fact that the charged fusion products (alpha particle) birth velocity is larger than the Alfvén velocity $V_A = B_T/\sqrt{4\pi\rho}$, where BT represents the toroidal magnetic field and ρ the plasma mass density[2,3]. Unstable Alfvén eigenmodes (AE) may redistribute alphas and reduce the ignition margins of a tokamak reactor and/or cause damage to the first wall. The destabilisation of AE[4] by the fusion-born alpha particles in tokamaks was first theoretically analysed in[5,6] and experimentally observed in TFTR[7]. The study of AE destabilisation by energetic ions produced by auxiliary heating, such as ion cyclotron resonant heating (ICRH)[8], is a valuable tool in understanding the physics issues related to Alfvén instabilities. These experiments offer the possibility of validating the models used in the extrapolation to reactor conditions[1].

In 1997, the first passive measurements of instabilities in the Alfvén frequency range were carried out at JET[9]. The new high frequency digital recorders were able to store 4 seconds of magnetic fluctuation data at a sampling frequency of 1MHz. With this system, detailed measurements of Alfvén instabilities have been done. It was observed that the Ion Cyclotron Resonant Heating (ICRH) driven energetic ions were able to destabilise Alfvén Eigenmodes (AE) at JET[10], for a wide range of plasma parameters. Under these conditions, a very complex Alfvén spectrum emerged and it has been a challenge to understand all the physics issues in detail. Nevertheless, a comprehensive picture of AE destabilisation by energetic ions has been established, with the aid of the Alfvén Eigenmode active diagnostic[11.12]. The present physics understanding can be summarised within the following topics: plasma equilibrium, alfvén wave propagation, particle orbits, wave particle interaction, energetic particle modes, non-linear behaviour, saturation amplitude and energetic particle redistribution and losses.

The reconstruction of the plasma equilibrium is the first and an important step in the detailed

modelling of AE. Usually, an accurate reconstruction of the safety factor (q) profile can be achieved using information from the sawteeth inversion radius or other MHD instabilities. However, the accurate equilibrium reconstruction of reversed shear scenarios at JET obtained with the use of lower hybrid current drive requires some further research. In particular scenarios with zero or negative current close to the axis[13]. However, using motion stark effect measurements together with the information from MHD instabilities, reasonably accurate inverted q profile equilibrium can be obtained.

The propagation of the Alfvén waves in toroidal plasmas is well established within the MagnetoHydroDynamics (MHD) framework, while both particle orbits and the wave particle interaction can be described successfully within the gyro-averaged approximation. In deep reversed shear scenarios, the orbits of energetic ions with energies in the 1MeV range are mostly in the non-standard regime, where the precession drift frequency is comparable with the poloidal bounce/ transit frequency. In this case, full orbit effects need to be retained, including non-standard potato orbits.

The study of the occurrence of energetic particle modes in plasmas with a significant fraction of energetic ions is also crucial. These modes have in general a higher fast ion instability threshold but once unstable can also have a larger impact on the confinement of energetic ions. It is, therefore, very important to understand the non-linear behaviour and saturation of these instabilities. Recent studies were able to describe in some detail the non-linear behaviour of AEs near to the instability threshold. It was possible to reproduce the pitchfork non-linear bifurcations observed in the experiments[14], the transition to the chaotic regime and chirping behaviour. The final step required for a precise prediction of the energetic ion confinement in a reactor is the calculation of energetic particle redistribution and loss due to unstable AE.

This paper will focus on the calculation of the AE spectrum, the interaction with the energetic ions and some aspects related to the physics of energetic particle modes. AE non-linear behaviour and the effect on particle confinement will not be addressed.

The modelling of AE instabilities in JET can be carried out using the CASTOR-K code[15]. The CASTOR-K code is a hybrid model, containing a fluid part for the propagation of AE and mode conversion to kinetic Alfvén waves, and a gyro-kinetic part for the interaction of the energetic ion with AE. After a brief description of the CASTOR-K model and some of the recent enhancements, the code will be used to analyse the damping of AE in Ohmic plasmas and the AE spectrum in deep reversed shear plasmas. The CASTOR-K model does not contain all the relevant aspects of the physics of the energetic particle modes, but some aspects, including the detailed interaction of EPMs with non-standard particle orbits, can be described using the present model.

2. CASTOR-K MODEL (FLUID PART)

The hybrid MagnetoDydroDynamic (MHD)-kinetic CASTOR model[16,17] solves the linearised resistive MHD equations in toroidal geometry, where the Finite Larmor Radius Effects and the

effect of the parallel electric field are included in the model within the Complex Resistivity approximation[18].

In the ideal MHD framework the damping of AE is dominated by continuum damping, caused by the resonant absorption of the AE energy at the Alfvén resonance[19]. This is due to the fact that the propagation of MHD waves in a non-uniform plasma becomes singular at the Alfvén resonance, yielding a continuous spectrum for a bounded plasma[20]. The continuum mode wave energy is absorbed at the Alfvén resonance layer due to phase mixing of the singular waves. In hot plasmas, the introduction of additional physics including non-ideal effects, such as finite perturbed electric field and finite Larmor radius, the Alfvén singularity is resolved. Non-ideal effects raise the order of the system of differential equations for AEs introducing new solutions which describe short wavelenght oscillations. The analysis of the higher order system of equations shows that the energy absorbed by phase mixing in ideal MHD is now converted into a new set of short wavelength modes. The parallel perturbed electric field and first order finite Larmor radius of core ions give the following correction to the vorticity equation[21]

$$\underbrace{(\vec{b}\times\vec{\nabla})(\nabla^2(\vec{b}\times\vec{\nabla})_\phi) + \nabla\left(\frac{\omega^2}{V_A^{\,2}}\nabla_\perp\phi\right)}_{Ideal\ \ MHD\ \ Port} + \underbrace{\frac{3}{4}\frac{\omega^2}{V_A^{\,2}}\rho_i^{\,2}\nabla^4{}_\perp\phi}_{FLR} + \underbrace{(1-i\delta_e)\frac{\omega^2}{V_A^{\,2}}\rho_s^{\,2}\nabla^4{}_\perp\phi + 0,}_{E_{||}>0\ Term}$$

with dissipation δ_e due to electron. The vorticity equation has the following form in resistive MHD

$$\underbrace{(\vec{b}\times\vec{\nabla})(\nabla^2(\vec{b}\times\vec{\nabla})_\phi) + \nabla\left(\frac{\omega^2}{V_A^{\,2}}\nabla_\perp\phi\right)}_{Ideal\ \ MHD\ \ Port} + \underbrace{(\vec{b}\times\vec{\nabla})\frac{i\eta}{4\pi\omega}(\nabla^4{}_\perp(\vec{b}\times\vec{\nabla})_\phi)}_{\text{Re}\ sistive\ Term} = 0$$

The direct comparison of the previous equations gives us the “complex resistivity”

$$\tilde{\eta} = 4\pi\omega\rho^2{}_s\left(\frac{2\omega}{\omega_A}\right)^2\delta_e + i4\pi\omega\left(\frac{3}{4}+\frac{T_e}{T_i}\right)\rho_i^{\,2}\left(\frac{2\omega}{\omega_A}\right)^2.$$

In order to understand the behaviour of Alfvén waves in the presence of FLR and finite parallel electric field, the Alfvén spectrum can be solved within the Wentzel-Kramers-Brillouin-Jeffreys (WKBJ) approximation. The transition from the resistive Alfvén spectrum into the kinetic Alfvén spectrum can be studied by changing the usual resistivity into a general complex parameter $\tilde{\eta}$. The fast varying solutions in the radial direction can be described accurately by the phase integral in the WKBJ approximation[22] $\phi \approx e^{\pm i\phi f}$, where $\frac{d\phi_r}{dr} = \sqrt{-\frac{\left(\vec{k}\times\vec{b}\right)+\omega^2}{\tilde{\eta}\omega}}$.

To obtain the WKBJ spectrum the following eigenvalue conditions for ω must be satisfied:

1) no anti-Stokes line crossings $\phi_f(b)-\phi_f(a) = p_\pi \rightarrow Im\,[\phi_f(a)] < 0 \wedge Im\,[\phi_f(b)] < 0$,

2) one at (a) and half at (b) anti-Stokes line crossings $\phi_f(a) = -p_\pi \rightarrow Im\,[\phi_f(b)] > 0$,

3) one at (b) and half at (a) anti-Stokes line crossings $\phi_f(b) = p_\pi \rightarrow Im\,[\phi_f(a)] > 0$,

where a,b are the boundaries.

In the generalised case of complex $\tilde{\eta}$ the spectrum rotates and the third branch disappears with the two remaining branches forming the kinetic Alfvén spectrum. The kinetic Alfvén waves corresponding to the second branch have a turning point at the Alfvén resonance giving origin to the Kinetic Toroidicity induced Alfvén Eigenmodes (KTAE) in toroidal geometry. The first branch does not have a turning point inside the plasma and play an important role in radiative damping of Alfvén waves. In the low shear ($s \rightarrow 0$) limit the dispersion relation for each branch take the form:

$$1)\ \frac{s+2\,(1+\omega^2)}{2\,(1+\omega^2)} = \sqrt{-\frac{\omega^2+1}{\tilde{\eta}\omega}} = p\pi;\ 2)\ \frac{s\omega^2+2i\,(1+\omega^2)}{2\tilde{\eta}\sqrt{\frac{\omega^2+1}{\tilde{\eta}\omega}}} = p\pi;\ 3)\ \left(1+\frac{s}{2}+2i\omega\right)\sqrt{-\frac{\omega^2+1}{\tilde{\eta}\omega}} = p\pi.$$

For very large values of p, $\omega = \frac{1}{2}\left(-\tilde{\eta}p^2\pi^2 \pm \sqrt{\tilde{\eta}^2p^4\pi^4-4}\right)$. Since p is the number of radial wave periods, $p \propto k_\perp$, one obtains $\gamma = \mathrm{Im}(\omega) \propto \tilde{\eta}k_\perp^{\,2}$, showing that within the CASTOR-K complex resistivity approximation the short wave length waves are damped proportionally to the perpendicular radial wave number square $k_\perp^{\,2}$.

The CASTOR-K code calculates the non-ideal Alfvén spectrum using two distinct numerical algorithms. In the first procedure the linearised non-ideal MHD equations are solved as an eigenvalue problem using inverse vector interaction. In the second method the plasma response to an external antenna excitation is calculated using linear solver. The damping of the eigenmode is determined by the width of the resonance or directly from the eigenvalue. The ideal and non-ideal plasma response for a simple benchmark cylindrical equilibrium[22] is shown in Fig. 1. As the non-ideal complex parameter $\tilde{\eta}$ increases the damping of the TAE located inside the toroidicity induced gap in the continuum increases, causing the resonance observed in the plasma response to broaden. The break up of the continuum in a discrete set of kinetic Alfvén waves is also clearly is visible in Fig. 1 as the non-ideal complex parameter $\tilde{\eta}$ is increased.

Numerical convergence for a JET limiter Ohmic discharge requires around 151 radial finite cubic elements and 11-17 poloidal Fourier harmonics, depending on edge q and toroidal mode number of the eigenmode.

Figure 2 shows the damping of n = 1 TAE mode as a function of the underlying plasma dissipation $\mathrm{Re}\,(\tilde{\eta}) \propto \delta_e$. Calculation of the damping of this mode shows that above a certain value of the underlying plasma dissipation δ_e, the damping becomes independent of the plasma dissipation δ_e

and depends only on the amount of energy converted from the AE to the runaway kinetic Alfvén wave. It is, therefore, shown that in this parameter regime the CASTOR-K model reproduces the radiative damping limit.

The analysis of the dependence of the damping of the TAE on the non-ideal parameter $\tilde{\eta}$ shows the existence of three separate cases that need to be considered. The damping of the TAE mode located at the bottom of the TAE gap tends to be dominated by radiative damping, which increases with $\tilde{\eta}$. The TAE mode located at the top of the gap usually crosses the Alfvén continuum and is continuum damped. This mode has a finite damping in ideal MHD and the damping has a weak dependence on $\tilde{\eta}$. KTAE modes do not exist in the ideal MHD and the damping decreases with $\tilde{\eta}$ as shown in Fig.3.

3.CASTOR-K MODEL (GYRO-KINETIC PART)

The Gyro-kinetic part of the CASTOR-K code calculates the transfer of energy between the fast particles and the mode. This code was originally developed in order to study TAE destabilisation by alpha particles, and later it was extended to analyse the influence of ICRH heated particles on the stability of lower frequency MHD modes.

The CASTOR-K code calculates then the contribution of the fast particles to the energy of the mode using a perturbative approach. It computes the first order perturbation on the eigenvalue due to the interaction between the wave and the energetic ion population. Using the eigenfunction determined by fluid part of the code. CASTOR-K decomposes the hot particle energy functional into poloidal bounce harmonics and integrates the contribution over the particle phase space, as seen in equation 1,

$$\delta\omega_{hot} = -\frac{2\pi^2}{\Omega m^2} \bullet_{\sigma} \!\!\!\!\!\!\int\!\!\!\!\!\!\int dp_{\phi} dE d\mu \bullet_{p=-\infty}^{\infty} \frac{\partial f}{\partial E} \frac{\tau_b |Y_p|^2 (\omega - n_0\omega^*)}{\omega + n_0\omega_D + p\omega_b}, \; Y_p = \oint \frac{d\tau}{\tau_b} L^{(1)} e^{ip\omega_b\tau} \quad (1).$$

P_ϕ represents the toroidal canonical momentum, μ the magnetic momentum, E the energy, L(1) the perturbed orbit Lagrangian, ω_* the diamagnetic frequency of the fast ions, ω perturbation frequency, ω_d toroidal precession drift frequency and ω_b the poloidal bounce frequency. The imaginary part of $\delta W_{HOT,}$, which represents contribution of the energetic ions to the linear MHD eigenvalue, is related to the growth rate of the mode (γ/ω) by

$$\frac{\gamma}{\omega} = \frac{1}{2\omega^2} \frac{Im[\delta W_{HOT}]}{E_k}, \quad (2)$$

where E_k is proportional to the mode energy and γ is the growth rate of the unperturbed mode, as shown in equation 2.

The six-dimension integration in phase space in performed using both numerical and analytic methods. In the original CASTOR-K version the integration was performed using the procedure represented in Table 1. The new version of the CASTOR-K code uses a modified procedure as

shown in table 2. The new procedure[24] assumes that ICRH transfers energy to the fast ions only the in perpendicular direction, generating distributions with a single value of the magnetic momentum divided by energy. This allows the energy integration to be performed numerically using the 2D binary search algorithm and the consequent calculation both the real and imaginary part of the quadratic form δW_{HOT}.

Table 1

	Variable		Integration Process
α	Gyro-angle	Analytical	Gyro-average
θ	Poloidal angle	Numerical	Fourier transform
ϕ	Toroidal angle	Analytical	Fourier Decomposition
E	Energy	Analytical	Pole Integration
μ/E	Magnetic Moment	Numerical	Binary Search
P_ϕ	Toroidal Momentum	Numerical	Binary Search

Table 2

	Variable		Integration Process
α	Gyro-angle	Analytical	Gyro-average
θ	Poloidal angle	Numerical	Fourier transform
ϕ	Toroidal angle	Analytical	Fourier Decomposition
E	Energy	Numerical	Binary Search
μ	Magnetic Moment	Analytical	ICRH distribution
P_ϕ	Toroidal Momentum	Numerical	Binary Search

The Binary Search Algorithm is important, because small "resonance" areas in phase-space dominate the wave-particle interaction. This algorithm allows consecutive mesh refinements in areas where the wave-particle interaction is strongest. In an initial step the algorithm surveys the entire phase-space, and in the following steps the mesh is refined using evaluation, ordering and storing procedures. The convergence is found to the linear in the number of steps and adequate in most practical applications.

4. ALFVÉN SPECTRUM EXCITED BY EXTERNAL ANTENNA IN OHMIC PLASMAS.

The calculated continuum and radiative damping were found to be very sensitive to the experimental profiles, in particular the density and safety factor profiles. However, using the destabilisation of the sawtooth as an evidence of the appearance of the q = 1 surface in the centre of the plasma, a relatively accurate q profile can be reconstructed for (Pulse No: 51158 at t = 16s) using the codes EFIT[25] and HELENA[26]. The density profile can also be reconstructed accurately using the

data from the LIDAR Thomson scattering and microwave interferometer diagnostics.

The calculated frequency and damping is compared with the measurements using the AE active excitation diagnostic. In this discharge, the probing frequency is scanned with the frequency range calculated to be in the vicinity of the Toroidicity induced gap. Once the system detects a resonance, it follows the mode measuring the frequency and damping as a function of time. In this discharge two n = 1 modes are found in the TAE gap. The MHD model also shows the existence of two n = 1 TAE modes in the gap in agreement with the experiments and the model is able to reproduce the frequency of the AEs with high accuracy as shown in Fig.4. The eigenfunctions calculated by the CASTOR for this discharge are shown in Figures 5,6. The radial plasma displacement is represented as a function of the normalised magnetic poloidal flux $s = \sqrt{\frac{\psi}{\psi_0}}$, which is approximately equivalent to the normalised plasma minor radius (r/a). The upper-frequency (f = 150-170kHz) TAE mode, shown in Fig.5, as no parity inversion, in contrast with the lower-frequency (f = 120-130kHz) TAE mode which has a parity inversion at s = 0.75. The calculated damping for the lower-frequency (f = 120-130kHz) TAE mode for this discharge is found to be 0.5%-1% a factor of 2 smaller than the measured damping of 1%-2% as shown in Fig.7.

5. ALFVÉN SPECTRUM IN DEEP REVERSED SHEAR PLASMAS

A detailed analysis of the Alfvén spectrum in deep reversed shear plasmas is carried out using an equilibrium reconstruction obtained with the MSE diagnostic at JET for Pulse No:49382. The reconstructed q profile is strongly reversed with q on axis q0~6.0 and q(min)~2.5 located around r(qmin)~0.62 minor radius. The Alfvén spectrum as calculated with the fluid part of the CASTOR-K code is quite complex and a number of eigenmodes have been found in the vicinity of the TAE gap. Among these, only three AEs with damping rate γ/ω less than 3% were found. The Alfvén continuous spectrum, the frequency and approximate location of the eigemodes found in the vicinity of the TAE gap are shown in Fig.8. A core localised EAE was found with frequency just above the TAE gap. The radial plasma displacement of the core localised EAE eigenfunction, represented as a function of the square root of the normalised magnetic poloidal flux, is shown in Fig.9. A global TAE exists in the middle of the TAE gap with small damping. The radial plasma displacement of the global TAE, represented as a function of the square root of the normalised magnetic poloidal flux, is shown in Fig.10. In addition, a localised eigenmode was found located in radius at the position of the minimum of q with frequency below the TAE mode frequency. The radial plasma displacement of this localised eigenmode, represented as a function of the square root of the normalised magnetic poloidal flux, is shown in Fig.11. The analysis of the frequency dependence on the evolution of q for these modes was carried out by varying the value of the minimum of q from 2.0 to 3.0. It was found that frequency of the mode located at the minimum of q was clearly linked with the tip of the Alfvén the continuum spectrum,

$$\frac{d}{dr}\left(k_{||}V_A\right) = 0$$

at the same position as shown in Fig.12. We conclude therefore that the Alfvén cascades observed in JET plasma with the deep reversed q-profiles, which were interpreted as an Energetic Particle Mode (EPM) located at position of q(min) and whose frequency is close to Alfvén continuous spectrum at position of q(min), can also exist in the absence of energetic ions, provided that the mode frequency is sufficiently close to the TAE gap. In the case of the frequency being far away from the TAE gap the mode existence requires finite pressure of energetic ions, therefore, this mode is referred to as an "EPM"-like mode.

In order to evaluate the stability of these modes in the presence of ICRH accelerated minority ions, it is required to take into account the orbits of high energy ions in deep reversed shear plasmas in some detail. In the small banana limit the particle orbits can be classified into passing and trapped particle. In the case of high-energy ions, where the banana width is comparable with the plasma minor radius the topology of the orbits is more complicated. Considering only the region in phase space relevant to ICRH accelerated minority ions the orbits can be classified in two groups, banana orbits and potato orbits. Due to the small current in the plasma core, a large fraction of ions with energies in the MeV range are in the potato regime and the toroidal precession drift frequency is comparable with the poloidal bounce frequency. Therefore, in the calculation of the destabilisation of AEs, it is crucial to take into account the contribution of non-standard orbits. For the configuration considered, it was found that the main destabilising influence is dominated by the trapped banana orbits, while most particles in the potato regime have a stabilising influence. Figure 13 represents the energy exchange between the energetic particles and the eigenmode localised around the position of q(min) as a function of the energy and the toroidal canonical momentum. The stabilising influence of mainly non-standard orbits is represented in red, while the destabilising influence of the trapped banana orbits is represented in blue. Stability diagram for the least damped eigenmodes calculated by the CASTOR-K code for the equilibrium of the deep reversed shear Pulse No:49382 is shown in Fig. 14. The TAE mode requires lower fast ion beta for instability but the mode localised at the minimum of q is the most unstable mode for a wider range of parameters. The overall stability analysis performed by the CASTOR-K code, where the EPM-like mode is shown to be the most likely unstable mode, is consistent with the experimental observation that Alfvén cascades are the dominant Alfvén instability in plasmas with deep reversed q-profiles.

Detailed comparison of the mode frequency pattern of the Alfvén Cascades and Alfvén continuum located at q(min) has been performed. The Alfvén continuum at q(min) behaviour is qualitatively the same as the Alfvén Cascades if only cases where Alfvén continuum has a maximum at the q(min) surface are considered. This is consistent with the existence of the mode near the TAE gap has calculated by the CASTOR-K code. Furthermore, quantitative good agreement is obtained by including a reduction of the mode frequency caused by the interaction with the energetic ions as shown in Fig.15. In the analysis the frequency of the mode is reduced by a factor inversely

proportional to the toroidal mode number, consistent with the limit where the fast particle orbit width is large compared with the mode width.

CONCLUSIONS

The CASTOR-K model for the radiative damping of TAE modes has been compared with the damping measurements performed at JET, using the AE active eigenmode excitation system. The mode frequency in Ohmic plasmas is reproduced by the ideal MHD model with great accuracy. The calculated damping was found to be around a factor of 2 smaller than the measured damping.

In deep reversed shear scenarios, a mode localised at the position of the minimum of the safety factor q was calculated by the CASTOR-K code. The mode was found to exist only if the frequency of the mode is close to the frequency of the TAE gap. Stability calculations show that this mode is the most unstable eigenmode for a wide range for parameters consistent with the experimental observation of Alfvén Cascades. The frequency pattern of the Alfvén Cascades is qualitatively in agreement with the time evolution of the Alfvén continuum at the location of q(min) which is linked to the frequency of the mode calculated by the CASTOR-K code. Measurements of these Alfvén instabilities are used to solve the inverse problem of identifying the plasma parameters, especially the safety factor (q).

REFERENCES

[1]. ITER Physics Basis chapter 5, Nuclear Fusion **39** (1999) 2471.
[2]. ROSENBLUTH, M.N. and RUTHERFORD, P.H., Phys. Rev. Lett. **34** (1975) 1428.
[3]. MIKHAILOVSKII, A.B., Sov. Phys. JETP **41** (1975) 890.
[4]. CHENG, C.Z., CHEN, L., CHANCE, M.S., Ann. Physics **161** (1985) 21.
[5]. CHEN, L., Theory of Fusion Plasmas- Proc. Joint Varenna-Laussane Int Workshop (Chexbres, Switzeland, 3-7 October 1988) ed J. Vaclavik, F. Troyon and E. Sindoni, p. 327
[6]. FU, G.Y. and VAN DAM, J.W., Phys. Fluids **B1** (1989) 1949.
[7]. WONG, K.L. et al, Phys. Rev. Lett. **66** (1991) 1874.
[8]. ALI-ARSHAD, S. and CAMPBELL, D., Plasma Phys. Control. Fusion **37** (1995) 715.
[9]. FASOLI, A. et al., Plasma Phys. Control. Fusion **39**, B287 (1997)
[10]. KERNER, W. et al, Nuclear Fusion **38** (1998) 1315.
[11]. FASOLI, A. et al, Nucl. Fusion **35** (1995) 1485.
[12]. FASOLI, A. et al, Nucl. Fusion **36** (1995) 258.
[13]. HAWKES, N. et al., Phys. Rev. Lett. **87**, 115001 (2001).
[14]. FASOLI, A. et al, Phys. Rev. Lett. **81**, (1998), 25
[15]. BORBA, D. and KERNER, W., J. Comput. Phys. **153**, 101 (1999).
[16]. KERNER, W. et al, Journal of Computational Physics **142**, (1998), 271
[17]. HUYSMANS, G.T.A. et al, Phys. Fluids **B5**, (1993), 1545
[18]. CONNOR, J., et al, 21th EPS Proceedings, Vol 18B Part II, 616, 1994,

[19]. VACLAVIK, J. and APPERT, K. Nucl. Fusion **31**, 1945 (1991).
[20]. GOEDBLOED, J.P. Phys. Fluids **18**, 1258 (1975).
[21]. CANDY, J. and ROSENBLUTH, M.N. Phys. Plasmas **1**, 356 (1994).
[22]. BORBA, D. et al Physics of Plasmas 1 (10), 3151, October 1994
[23]. JAUN, A. et al, Plasma Phys. Control. Fusion 39 (1997) 549
[24]. NABAIS, F. et al, 8 th European fusion theory conference 1999, Como, Italy
[25]. LAO, L et al., Nuclear Fusion **30** (1990) 1035
[26]. HUYSMANS, G.T.A et al Phys. Fluids B **3** (6), 1506 (1992)

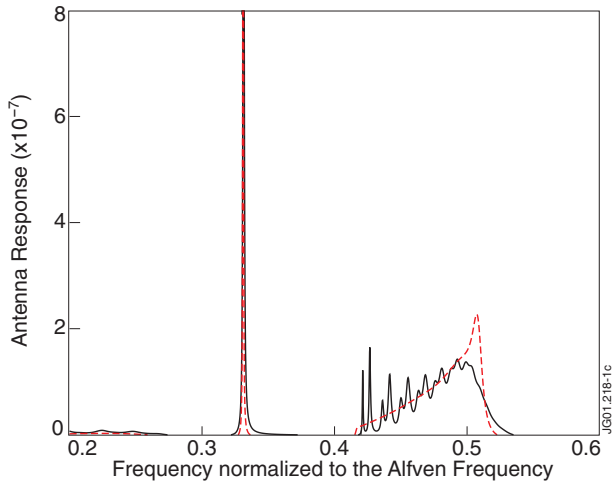

Figure 1: Ideal (red-dashed) and non-ideal (black) plasma response for a simple benchmark cylindrical equilibrium, showing the increase in damping of the TAE located inside the continuum gap and the break up of the continuum in a discrete set of kinetic Alfvén waves as the complex parameter is increased.

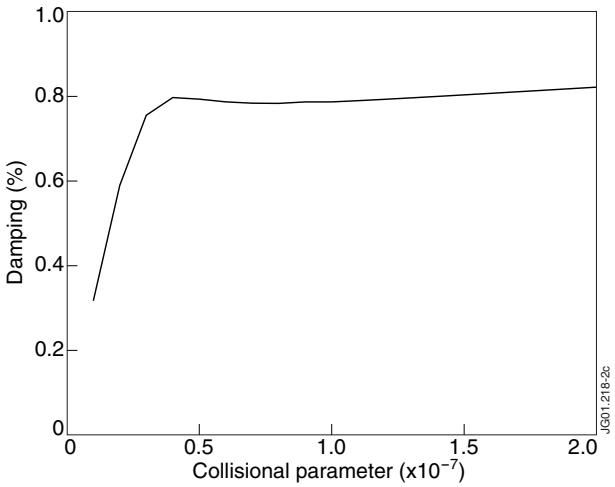

Figure 2: Damping of n=1 TAE mode as a function of the underlying plasma dissipation. Above a certain value of dissipation the overall damping becomes independent of the underlying plasma dissipation, reproducing the radiative damping limit.

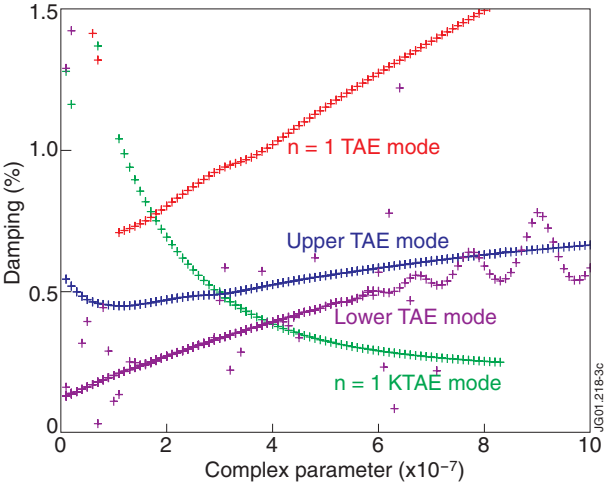

Figure 3: Damping of n=1 TAE and KTAE modes as a function of the non-ideal complex parameter. The damping of TAEs mode increases with plasma pressure, directly related non-ideal complex parameter, while the damping of KTAE mode decreases with plasma pressure.

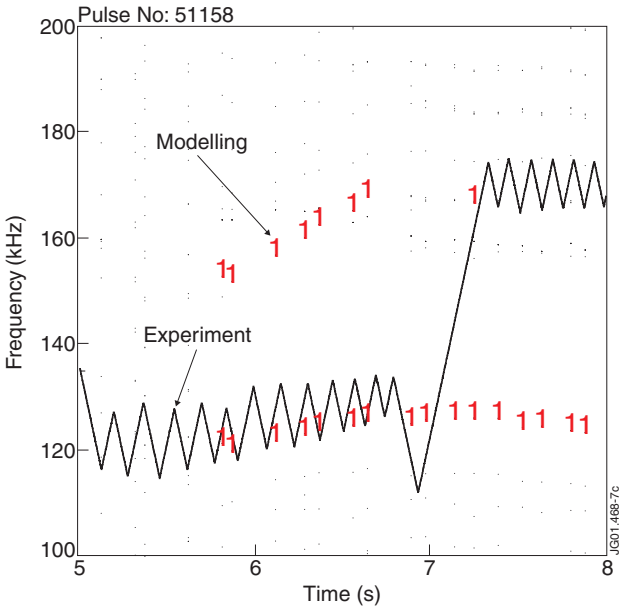

Figure 4: Frequency of two TAE modes (lower TAE, upper TAE) measured using the active AE excitation diagnostic at JET (continuous line), compared with the frequency calculated using the CASTOR code (symbol 1) for Pulse No: 51158. The MHD model reproduces the experimentally observed frequency with high accuracy.

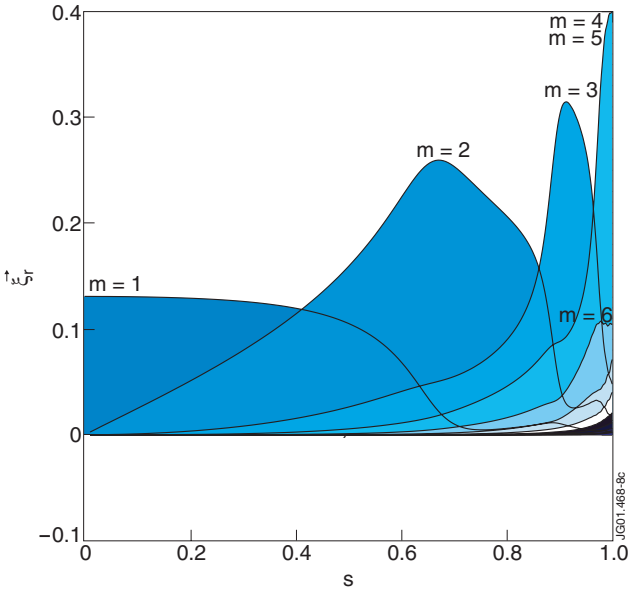

Figure 5: Radial plasma displacement as a function of the square root of the normalised poloidal magnetic flux of the upper-frequency (f=150-170kHz) TAE mode calculated using the CASTOR code for Pulse No: 51158.

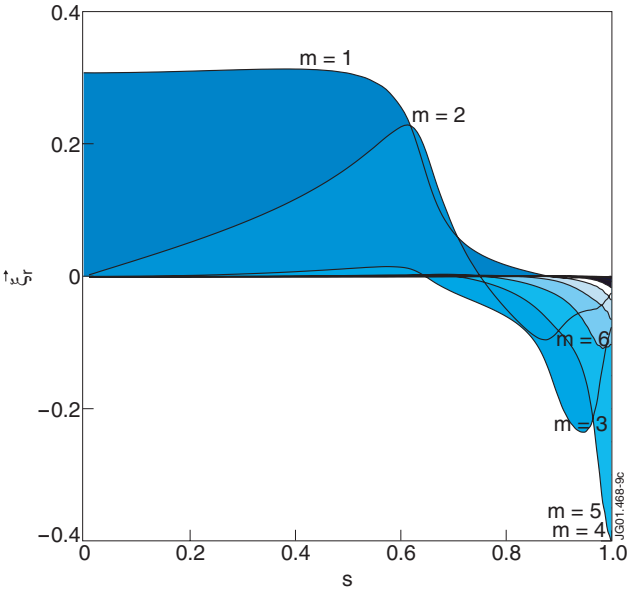

Figure 6: Radial plasma displacement as a function of the square root of the normalised poloidal magnetic flux of the lower-frequency (f=120-130kHz) TAE mode calculated using the CASTOR code for Pulse No: 51158.

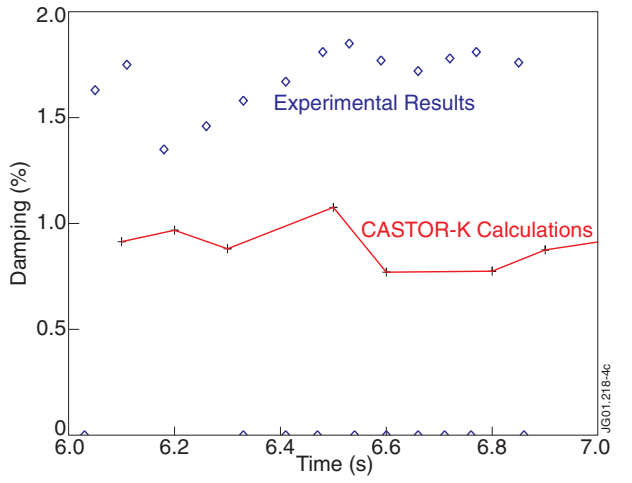

Figure 7: Comparison between the TAE damping measured by the active AE antenna system and the damping calculated using the CASTOR-K code for Pulse No: 51158, for the lower-frequency (f=120-130kHz) TAE mode. The calculated damping for the lower TAE mode for this discharge is found to be 0.5%-1% a factor of 2 smaller than the measured damping of 1%-2%.

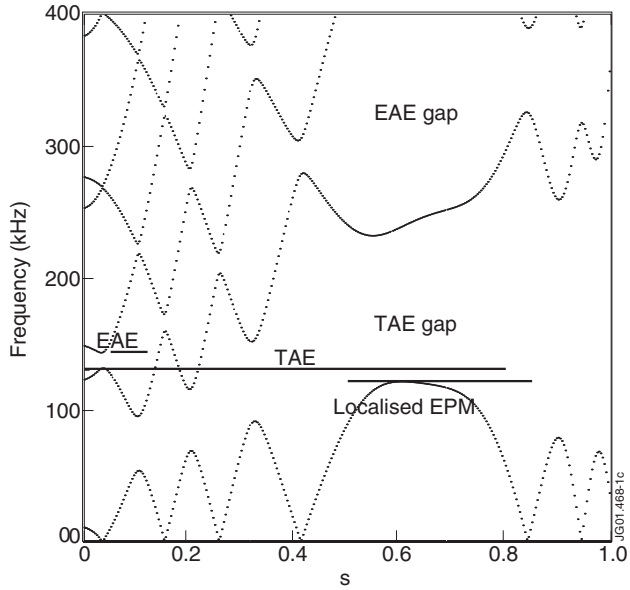

***Figure 8:** Alfvén continuous spectrum, the frequency and approximate locating of the eigemodes found in the vicinity of the TAE gap for the deep reversed shear Pulse No: 49382. A global TAE exists in the middle of the TAE gap and a core localised EAE is found with frequency just above the TAE gap. In addition, a localised eigenmode is found located in radius at the position of the minimum of q with frequency below the TAE mode frequency.*

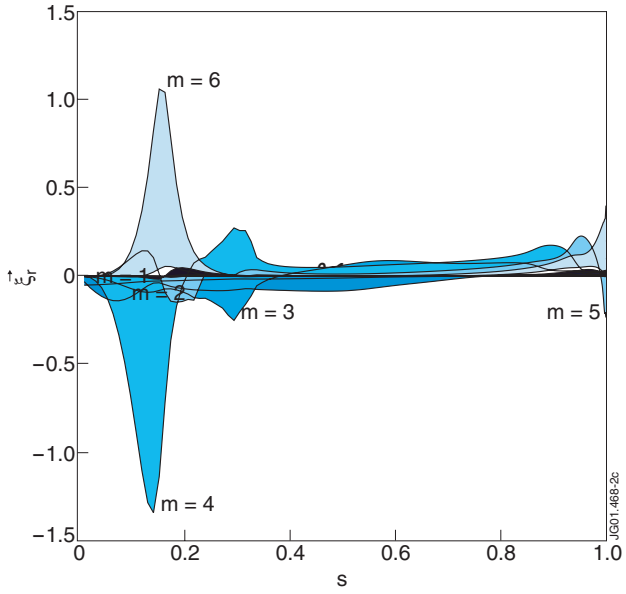

Figure 9: Radial plasma displacement as a function of the square root of the normalised poloidal magnetic flux of a core localised EAE with frequency just above the TAE gap for the deep reversed shear Pulse No: 49382.

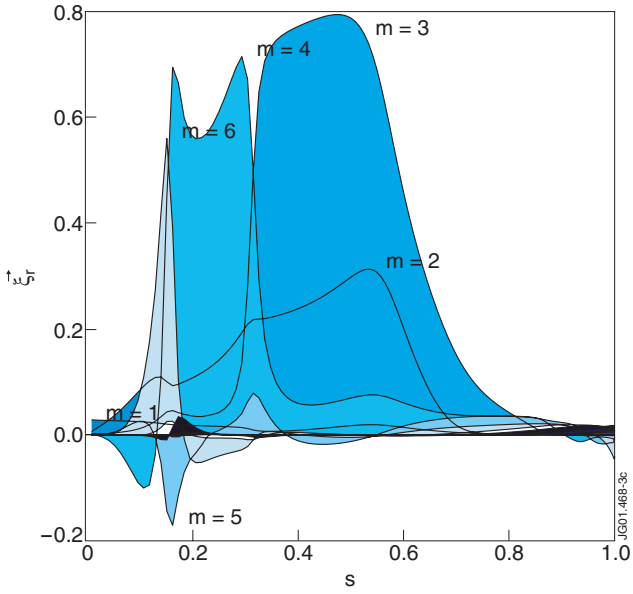

Figure 10: Radial plasma displacement as a function of the square root of the normalised poloidal magnetic flux of a global TAE that exists in the middle of the TAE gap for the deep reversed shear Pulse No: 49382.

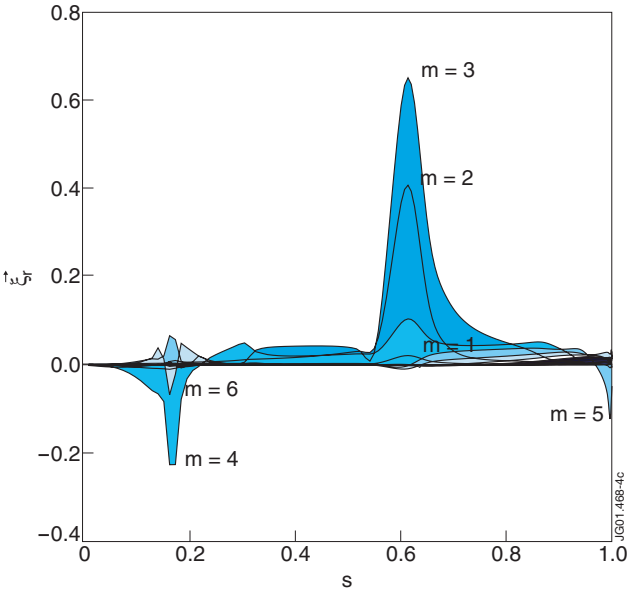

Figure 11: The radial plasma displacement as a function of the square root of the normalised poloidal magnetic flux of a localised eigenmode found localised in radius at the position of the minimum of q with frequency below the TAE mode frequency for the deep reversed shear Pulse No: 49382.

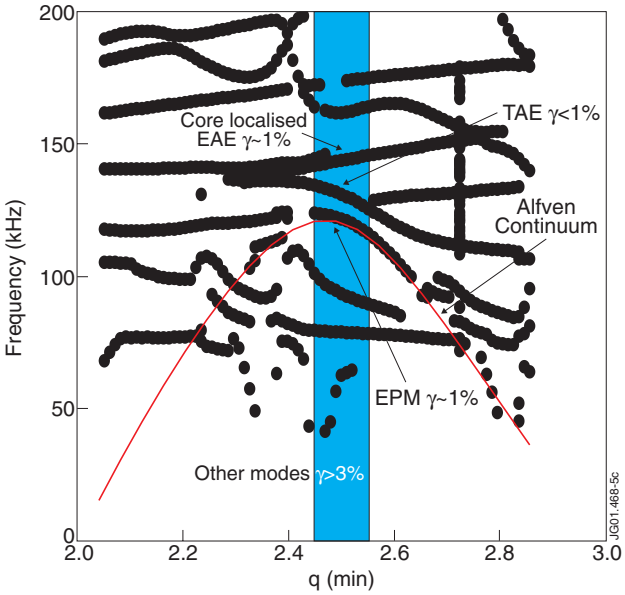

Figure 12: Analysis of the frequency dependence on the evolution of q of the Alfvén spectrum by varying the value of the minimum of q from 2.0 to 3.0. The Alfvén continuum at the position of q(min) is represented by the red line. The eigenmodes with the calculated damping smaller than 1% are also indicated in the figure. The frequency of the mode located at the minimum of q is clearly liked with the continuum spectrum at the same position.

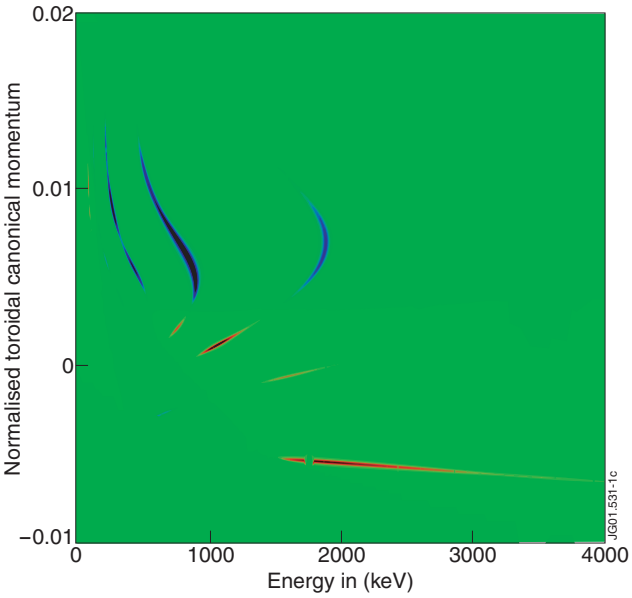

Figure 13: Energy exchange between the energetic particles and the eigenmode localised around the position of q(min) as a function of the energy and the toroidal canonical momentum. The stabilising influence of mainly non-standard orbits is represented in red, while the destabilising influence of the trapped banana orbits is represented in blue.

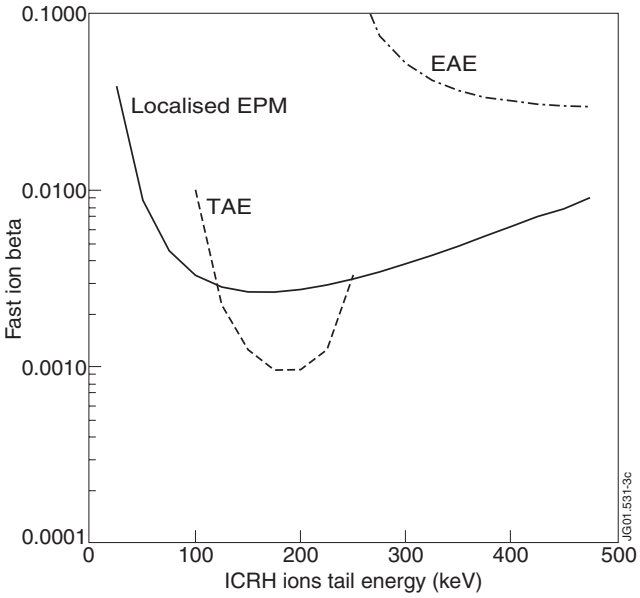

Figure 14: Stability diagram for the least damped eigenmodes calculated by the CASTOR-K code for the equilibrium of the deep reversed shear Pulse No: 49382. The TAE mode requires lower fast ion beta for instability but the mode localised at the minimum of q is the most unstable for a wide range of parameters.

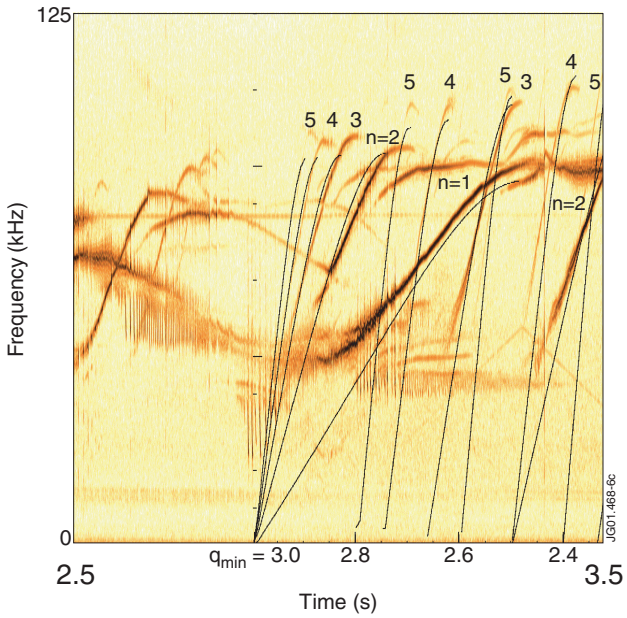

Figure 15: Spectrogram of the magnetic fluctuations showing the presence of Alfvén cascades common in deep reversed shear discharges with ICRH. The calculated frequency of the Alfvén continuum at the position of q(min) modified in order to account for the presence of fast particles is shown for comparison.